AMERICAN SOCIETY FOR MICROBIOLOGY | Journal of Virology®

PATHOGENESIS AND IMMUNITY

Directed Evolution of an Influenza Reporter Virus To Restore Replication and Virulence and Enhance Noninvasive Bioluminescence Imaging in Mice

Hui Cai,[a] Meisui Liu,[b] Charles J. Russell[a,c,d]

[a]Department of Infectious Diseases, St. Jude Children's Research Hospital, Memphis, Tennessee, USA
[b]Arts and Sciences, Brandeis University, Waltham, Massachusetts, USA
[c]Centers of Excellence for Influenza Research and Surveillance (CEIRS), Memphis, Tennessee, USA
[d]Department of Microbiology, Immunology and Biochemistry, College of Medicine, The University of Tennessee Health Science Center, Memphis, Tennessee, USA

ABSTRACT Reporter viruses provide a powerful tool to study infection, yet incorporating a nonessential gene often results in virus attenuation and genetic instability. Here, we used directed evolution of a luciferase-expressing pandemic H1N1 (pH1N1) 2009 influenza A virus in mice to restore replication kinetics and virulence, increase the bioluminescence signal, and maintain reporter gene expression. An unadapted pH1N1 virus with *NanoLuc luciferase* inserted into the 5′ end of the PA gene segment grew to titers 10-fold less than those of the wild type in MDCK cells and in DBA/2 mice and was less virulent. For 12 rounds, we propagated DBA/2 lung samples with the highest bioluminescence-to-titer ratios. Every three rounds, we compared *in vivo* replication, weight loss, mortality, and bioluminescence. Mouse-adapted virus after 9 rounds (MA-9) had the highest relative bioluminescence signal and had wild-type-like fitness and virulence in DBA/2 mice. Using reverse genetics, we discovered fitness was restored in virus rPB2-MA9/PA-D479N by a combination of PA-D479N and PB2-E158G amino acid mutations and *PB2* noncoding mutations C1161T and C1977T. rPB2-MA9/PA-D479N has increased mRNA transcription, which helps restore wild-type-like phenotypes in DBA/2 and BALB/c mice. Overall, the results demonstrate that directed evolution that maximizes foreign-gene expression while maintaining genetic stability is an effective method to restore wild-type-like *in vivo* fitness of a reporter virus. Virus rPB2-MA9/PA-D479N is expected to be a useful tool for noninvasive imaging of pH1N1 influenza virus infection and clearance while analyzing virus-host interactions and developing new therapeutics and vaccines.

IMPORTANCE Influenza viruses contribute to 290,000 to 650,000 deaths globally each year. Infection is studied in mice to learn how the virus causes sickness and to develop new drugs and vaccines. During experiments, scientists have needed to euthanize groups of mice at different times to measure the amount of infectious virus in mouse tissues. By inserting a foreign gene that causes infected cells to light up, scientists could see infection spread in living mice. Unfortunately, adding an extra gene not needed by the virus slowed it down and made it weaker. Here, we used a new strategy to restore the fitness and lethality of an influenza reporter virus; we adapted it to mouse lungs and selected for variants that had the greatest light signal. The adapted virus can be used to study influenza virus infection, immunology, and disease in living mice. The strategy can also be used to adapt other viruses.

KEYWORDS influenza virus, reporter virus, bioluminescence, mouse adaptation, noninvasive imaging

Received 6 April 2018 **Accepted** 6 June 2018
Accepted manuscript posted online 13 June 2018
Citation Cai H, Liu M, Russell CJ. 2018. Directed evolution of an influenza reporter virus to restore replication and virulence and enhance noninvasive bioluminescence imaging in mice. J Virol 92:e00593-18. https://doi.org/10.1128/JVI.00593-18.
Editor Terence S. Dermody, University of Pittsburgh School of Medicine

Address correspondence to Charles J. Russell, charles.russell@stjude.org.

Bioluminescence imaging of viral infection provides a powerful tool to investigate virus-host interactions, yet inserting luciferase into a negative-strand RNA genome typically attenuates replication and virulence. *In vivo* infection dynamics have classically been measured by determining the titer of infectious virus recovered from euthanized animals or respiratory washes. In contrast, bioluminescence imaging measures in living animals the expression of luciferase, a marker for the extent of infected cells. Longitudinal measurement of infection reduces the number of animals needed and interanimal variability, increases the practical number of time points observed, assists long-term measurement of chronic infection, and enables measurement of both primary infection and reinfection in the same animal (1, 2). For members of the order *Mononegavirales*, reporter genes are often inserted as additional transcriptional units (3). However, luciferase-expressing Sendai virus and respiratory syncytial virus (RSV) either have been attenuated in mice due to resultant alterations in reporter gene expression (4, 5) or have not yet been compared to parental wild-type (WT) strains *in vivo* (6–8). Influenza A viruses, from the family *Orthomyxoviridae*, contain 8 gene segments (9). Luciferase insertions have been introduced into *PB2* (7, 10), *PB1* (11, 12), *PA* (13–16), and *NA* (17) genes, in addition to an *NS-PB1* rearrangement (18, 19). Influenza reporter viruses must retain gene-packaging sequences at the termini and need to be relatively small due to the relatively small size (~0.9 to 2.4 kb) of the gene segments (20). Numerous luminescent and fluorescent influenza viruses have reduced replication kinetics and attenuated virulence due to altered gene expression, disrupted splicing, attenuation, or genetic instability (10, 17–19, 21–28). Thus, strategies to restore reporter virus fitness are needed to noninvasively study viral spread, clearance, and pathogenesis and to develop novel antivirals and vaccines.

Expected mechanisms of attenuation can be reduced or eliminated during initial construction by incorporating a compensatory enhancement. Inserting an additional transcriptional unit into the Sendai virus genome attenuates replication by decreasing expression of downstream viral genes and altering the ratio of viral gene expression (29). Wild-type Sendai virus contains a suboptimal transcription start sequence upstream of the *fusion* (*F*) gene (30), which can be repaired when inserting the firefly luciferase gene into the M-F gene junction to yield a bioluminescent Sendai virus with wild-type-like replication and virulence in mice (4). In an alternative approach, disruption of Sendai viral gene expression was also avoided by expressing *Renilla* luciferase from an internal ribosome entry site (IRES) engineered into the existing *nucleocapsid* (*N*) transcriptional unit (31). In the case of influenza viruses, which have multiple compact gene segments containing terminal packaging sequences, large insertions are often not genetically stable (25, 26, 28), and insertions at either end of the coding region can disrupt virus assembly (32, 33). Limitations on insertion size can be addressed by selecting a relatively small reporter gene, such as the NanoLuc (Nluc) luciferase gene (*NanoLuc* [*Nluc*]) (15), which is relatively small (19-kDa) and has ~150-fold greater light output than firefly and *Renilla* luciferases (34). Of course, gene-packaging sequences need to be added to insertions at the 3′ and 5′ termini (10, 11, 13-17, 35). Multiple reporter gene candidates can be created and compared in parallel or in an iterative manner to counteract attenuation (14, 15). If engineering strategies are unable to adequately restore reporter viral fitness for *in vivo* infections, a reporter virus can be blind adapted by passaging virus recovered from mouse lungs (36).

The goal of the present study was to generate a bioluminescent reporter virus that was nonattenuated in mice to visualize infection and clearance of the 2009 pandemic H1N1 (pH1N1) influenza virus, which now circulates seasonally. In general, seasonal influenza viruses are estimated to contribute to 291,000 to 645,000 deaths worldwide annually (37). Higher mortality rates are associated with influenza pandemics and less effective seasonal vaccine formulations (38). We generated the rTN09-PA-Nluc virus containing a *NanoLuc* fusion in the 5′ end of the *PA* gene of A/TN/1-560/2009 (H1N1). This strategy was previously used to generate luciferase reporter viruses in the genetic backgrounds of A/WSN/33 and A/CA/04/2009 H1N1 strains, A/Vietnam/1203/2004 (H5N1), and A/Anhui/01/2013 (H7N9) (13, 15, 16). In our preliminary studies, rTN09-PA-

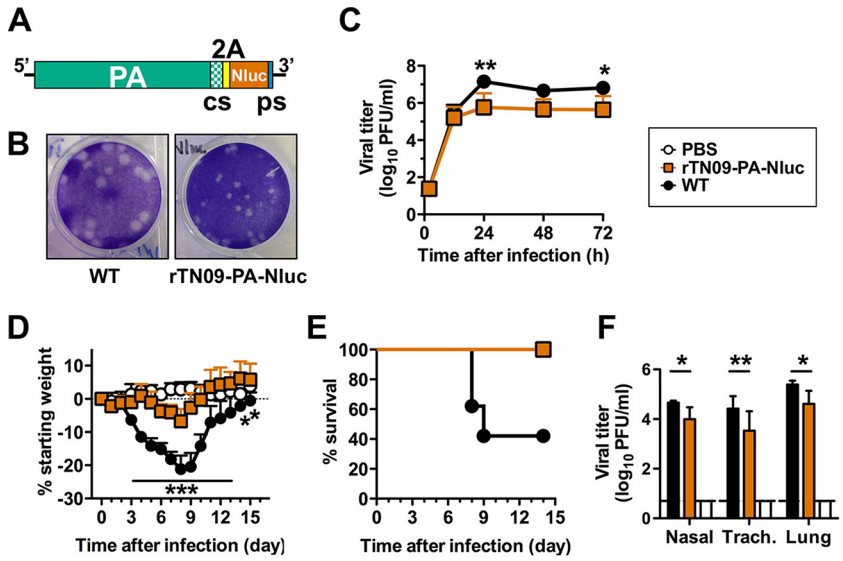

FIG 1 rTN09-PA-Nluc H1N1 influenza virus is attenuated in MDCK cells and mice. (A) Schematic representation of the PA-Nluc cDNA. The codon swap (cs) region, self-cleaving 2A peptide, *NanoLuc luciferase* (*Nluc*), and packaging sequence (ps) are indicated. (B) Plaque morphologies of WT and rTN09-PA-Nluc after 2 days of infection in MDCK cells at 37°C. (C) Multistep replication kinetics of WT and rTN09-PA-Nluc in MDCK cells. MDCK cells were infected at an MOI of 0.001, and culture supernatants were collected at the indicated times and titrated by plaque assay in MDCK cells. (D and E) Body weight changes (D) and survival (E) were monitored daily for mice intranasally inoculated with 30 μl PBS containing 750 PFU of WT or rTN09-PA-Nluc. (F) Nasal turbinates, trachea, and lungs were harvested from the mice 4 days postinfection (dpi), and virus titers in tissue homogenates were determined by plaque assay. The reported values are means and standard deviations ($n = 5$). *, $P < 0.05$; **, $P < 0.01$; ***, $P < 0.001$.

Nluc was attenuated. We subsequently tested the hypothesis that *in vivo* replication and virulence of rTN09-PA-Nluc could be restored without compromising reporter gene expression and stability by using a directed-evolution approach whereby virus samples are passaged in murine lungs and are selected in each round based on having the highest ratio of *in vivo* bioluminescence to infectious viral titer.

RESULTS

Attenuated rTN09-PA-Nluc reporter virus. To generate a recombinant pH1N1 reporter virus that expresses Nluc, we adopted the strategy of Mehle and coworkers (13, 15, 16). In the 3′ end of the cDNA (5′ end of the viral RNA) of the PA gene segment of A/TN/1-560/2009 (H1N1), we made synonymous mutations to codons located in the packaging sequence and appended in tandem a 2A cleavage sequence, the *Nluc* gene, and the *PA* packaging sequence (Fig. 1A). We generated by reverse genetics the reporter virus rTN09-PA-Nluc using the engineered PA cDNA plasmid and wild-type cDNA plasmids for the remaining seven gene segments. Compared to wild-type virus generated by reverse genetics, r.g.-A/TN/1-560/2009 (H1N1), rTN09-PA-Nluc formed smaller plaques and yielded 10-fold less infectious virus in MDCK cells (Fig. 1B and C). In groups of DBA/2 mice inoculated intranasally with 750 PFU virus in 30 μl, the wild type induced a mean maximum weight loss of approximately 21% and a mortality of 60% (Fig. 1D and E). In the rTN09-PA-Nluc group, mean maximal weight loss was reduced to approximately 7%, and all animals survived infection. In parallel groups, respiratory tissues were collected 4 days after inoculation and plaque titrated. Viral loads in mice infected with rTN09-PA-Nluc were approximately 10-fold lower than in those infected with the wild type (Fig. 1F).

Mouse-adapted reporter viruses. To restore the fitness of rTN09-PA-Nluc, we passaged lung-harvested virus 12 times in groups of five DBA/2 mice. The inoculated doses were decreased stepwise as follows: 5,000 PFU during rounds 1 to 3, 1,000 PFU during rounds 4 to 6, 200 PFU during rounds 7 to 9, and 50 PFU during rounds 10 to

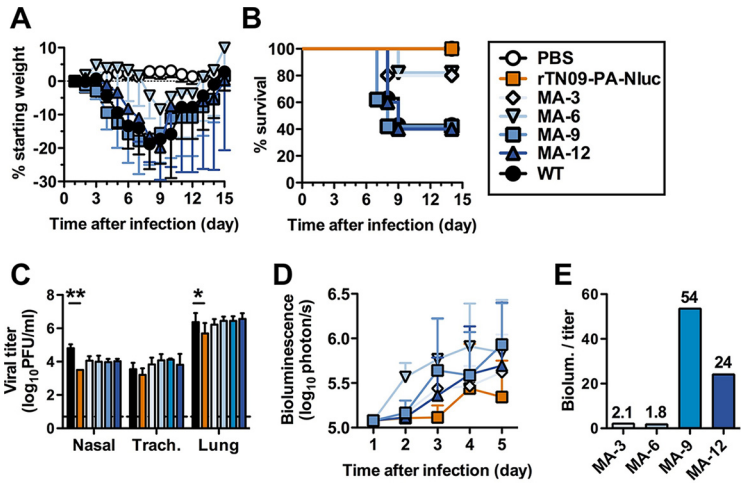

FIG 2 Mouse-adapted reporter viruses restore virus replication and virulence in mice. Groups of 5 DBA/2 mice were intranasally inoculated with 30 μl PBS containing 750 PFU of virus. (A and B) Body weight changes (A) and survival (B) were observed for 14 days in intact mice. (C) Virus tissue titers in nasal turbinates, trachea, and lungs were measured 4 dpi. (D) Noninvasive bioluminescence intensities in the lungs were observed for 5 days in intact mice. (E) The bioluminescence/titer ratios at 4 dpi were calculated for the four mouse-adapted (MA) variants. The reported values are means and standard deviations ($n = 5$). *, $P < 0.05$; **, $P < 0.01$.

12. Four days after inoculation, we measured *in vivo* bioluminescence and harvested lung tissue for plaque titration. Each round, we propagated virus into three naive mice from the mouse with the highest bioluminescence-to-titer ratio and into two naive mice from the mouse with the second-highest ratio. We used this selection criterion to avoid propagating virus lacking the reporter gene. After 12 passages, we intranasally inoculated groups of DBA/2 mice with 750 PFU of virus yielded after 3, 6, 9, and 12 rounds of adaptation in mouse lungs. We designated the viruses MA-3, MA-6, MA-9, and MA-12, respectively. The wild type caused a mean maximum weight loss of approximately 19% and a mortality of 60%, while MA-3 and MA-6 were attenuated (Fig. 2A and B). MA-9 and MA-12 caused 60% mortality, like the wild type, and induced similar mean maximal weight loss (approximately 18% and 20%, respectively). Four days after infection, MA-9 and MA-12 also had lung and tracheal viral loads similar to those of the wild type (Fig. 2C). The mean nasal viral load for the wild type was approximately 4.8 $\log_{10}$ units, while those of MA-9 and MA-12 were reduced to approximately 4.0 $\log_{10}$ units. Consistent with increased replication in DBA/2 mice compared to unadapted rTN09-PA-Nluc, the mouse-adapted viruses had increased *in vivo* bioluminescence values (Fig. 2D). MA-9 had the highest bioluminescence-to-titer ratio (Fig. 2E) and was selected for further characterization.

MA-9 mutations restoring fitness. We plaque titrated MA-9 lung homogenate and picked 29 plaques. For each of the 29 virus clones, we amplified one round in MDCK cells and measured *in vitro* fitness by plaque titration and plaque size. Virus titers ranged from 20 to 430,000 PFU (data not shown). We inoculated groups of five DBA-2 mice with the 10 clones having the highest titers in MDCK cells, and we selected the four clones causing the greatest weight loss (MA9-1, MA9-2, MA9-15, and MA9-22). In a separate experiment, these four clones caused weight loss similar to that with wild-type virus and the parental MA-9 (Fig. 3A). The wild type and MA9-2 caused 40% mortality, MA9-1 and MA9-22 caused 50% mortality, and MA9-15 caused 100% mortality (Fig. 3B). All four clones had lung and tracheal viral loads similar to those of wild-type virus and the parental MA-9 (Fig. 3C). As with the parental MA-9, the nasal viral loads of the four clones were approximately 10-fold lower than that of the wild type. MA9-22 was selected for sequencing and subsequent analyses because it had weight loss, mortality, and lung titers similar to the wild type and had average *in vivo* bioluminescence values similar to those of the parental MA-9 (Fig. 3D). MA9-1 and

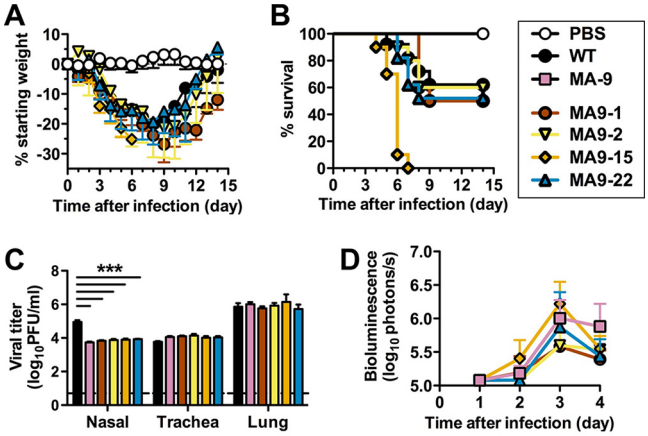

FIG 3 Mouse-adapted virus MA9-22 has restored fitness in DBA/2J mice. Groups of 5 DBA/2 mice were intranasally inoculated with 30 μl PBS containing 750 PFU of virus. (A and B) Body weight changes (A) and survival (B) were observed for 14 days in intact mice. (C) Virus tissue titers in nasal turbinates, trachea, and lungs were measured 4 dpi. (D) Noninvasive bioluminescence intensities in the lungs were observed for 4 days in intact mice. The ratio of bioluminescence/titer at 4 d.p.i. was calculated for the four mouse-adapted (MA) variants. In all panels, the reported values are means $\pm$ standard deviations (n = 5) and symbols are PBS (white circles), WT (black circles), MA-9 (pink squares), MA9-1 (brown circles), MA9-2 (yellow triangles), MA9-15 (orange diamonds), and MA9-22 (blue triangles). ***, $P < 0.001$.

MA9-2 had lower peak bioluminescence values than MA9-22. MA9-15 caused greater mortality than the wild type and was not further characterized due to a pause in gain-of-function research that has since been discontinued.

Sequencing of MA9-22 revealed no mutation in the HA, NA, and NS gene segments. The NP segment contained two synonymous mutations in its coding region, and the M and PB1 segments had one synonymous mutation (Table 1). These four synonymous mutations were not investigated further. Instead, we focused on the *PA-Nluc* and *PB2* genes, each of which contained two synonymous mutations and one amino acid mutation. All the mutations were outside the gene-packaging sequences (Table 1 and Fig. 4A and B). PA-Nluc contained a D479N amino acid mutation and synonymous mutations at nucleotides 1689 and 2127 (Fig. 4A). One of 10 PA-Nluc clones from MA9-22 also contained an F520Y mutation (Table 1). The F520Y mutation was not studied further because of its low abundance. PB2 contained an E158G amino acid mutation and synonymous mutations at nucleotides 1161 and 1977 (Fig. 4B).

We attempted to rescue a variety of viruses containing individual mutations or combinations of mutations in the *PA-Nluc* and *PB2* genes (Table 2). With respect to the amino acid mutations, we were unable to rescue rPB2-E158G in 10 attempts but

TABLE 1 Nucleotide changes in clone MA9-22

Gene	Nucleotide position	Mutation
PB2	473	A/G (E158G)
	1161	C/T
	1977	C/T
PB1	1110	A/G
PA-Nluc	1435	G/A (D479N)
	1559	T/A (F520Y)[a]
	1689	A/G
	2127	C/A
NP	814	C/T
	903	G/A
M	618	T/C

[a]Found in only 1 clone out of 5.

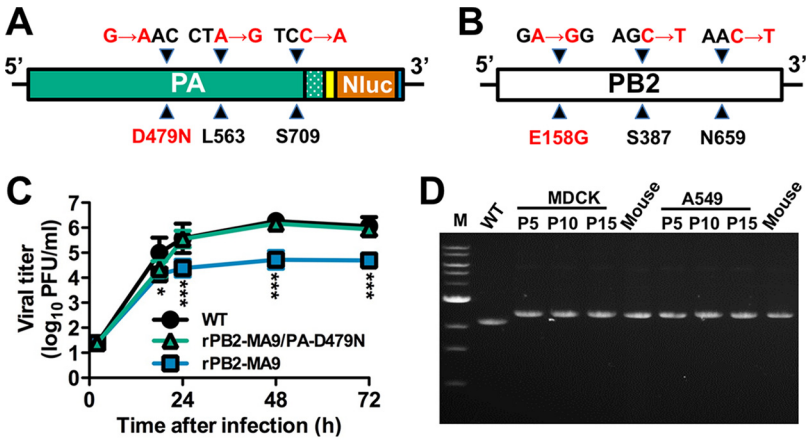

FIG 4 MA9-22 mutations in *PA* and *PB2* genes and their influence on MDCK replication kinetics and reporter insert stability. (A and B) Nonsynonymous amino acid mutations and synonymous nucleotide substitutions in MA9-22 *PA* (A) and *PB2* (B) genes. Nucleotide mutations are listed above the genes, and amino acid mutations are below. (C) Multistep replication kinetics of WT, rPB2-MA9, and rPB2-MA9/PA-D479N in MDCK cells infected at an MOI of 0.01 PFU/cell. The reported values are means and standard deviations of the results of 3 independent experiments. *, $P < 0.05$; ***, $P < 0.001$. (D) *PA-Nluc* gene stability after multiple passages in cell culture (MDCK or A549 cells) and after passage in cell culture followed by infection in DBA/2 mice. RT-PCR was performed on RNA isolated from WT stock virus, three viral stocks after passage in MDCK and A549 cells (P5, P10, and P15), and day 4 mouse lung homogenates of virus previously passaged 5 times in MDCK cells (Mouse, left) or A549 cells (Mouse, right). The PCR product was analyzed by 0.7% agarose gel electrophoresis using primers that flank the reporter gene. M, molecular weight DNA ladder.

recovered rPA-D479N and the double mutant rPB2-E158G/PA-D479N. With respect to viruses containing synonymous and nonsynonymous mutations, we were unable to rescue rPA-MA9, a virus containing all three mutations in the *PA* gene. We were able to generate rPB2-MA9, which had all three PB2 mutations, and rPB2-MA9/PA-D479N.

To identify mutations contributing to *in vivo* fitness and pathogenicity, we inoculated groups of DBA/2 mice with 750 PFU or BALB/c mice with 5,000 PFU using the viruses listed in Table 2. We monitored weight loss, survival, and bioluminescence in living mice. In parallel groups, we collected respiratory tissues after 4 days of infection to measure viral loads. Similar to the unadapted reporter virus (rTN09-PA-Nluc), in DBA/2 mice, rPA-D479N and rPB2-E158G/PA-D479N permitted 100% survival, caused approximately 10% weight loss or less, and had lung viral loads at least 0.7 $\log_{10}$ units lower than those of the wild type (Table 2). Thus, the PA mutation D479N did not restore fitness when present alone or in combination with the PB2 mutation E158G. rPB2-MA9 had weight loss, mortality, and lung viral loads comparable to those of the wild type in DBA/2 mice (Fig. 5 and Table 2) but grew to a level approximately 1 $\log_{10}$ unit lower in MDCK cells (Fig. 4C) and approximately 1.5 $\log_{10}$ units lower in DBA/2 nasal and tracheal homogenates (Fig. 5C). Addition of the PA-D479N mutation to

TABLE 2 Virus properties in DBA/2 mice

Recombinant virus	Rescue frequency	Survival	Max % wt loss[a]	Lung titer[b]
WT	2/2	4/10	21.7 ± 7.2	5.1 ± 0.1
rTN09PANluc	2/2	5/5	6.7 ± 3.4	4.1 ± 0.3
rPB2-E158G	0/10	ND[c]	ND	ND
rPA-D479N	2/2	5/5	8.1 ± 4.5	4.4 ± 0.3
rPB2-E158G/PA-D479N	1/4	5/5	10.2 ± 5.4	4.3 ± 0.2
rPB2-MA9	2/2	2/10	23.5 ± 8.3	4.8 ± 0.1
rPB2-MA9/PA-D479N	2/2	0/10	26.7 ± 1.3	5.4 ± 0.1

[a]The maximum change in the mean value (percentage) ± standard deviation observed over a period of 14 days postinoculation.
[b]Lung titer ($\log_{10}$ PFU/ml) was determined 4 days postinoculation.
[c]ND, not determined because virus was not rescued by reverse genetics.

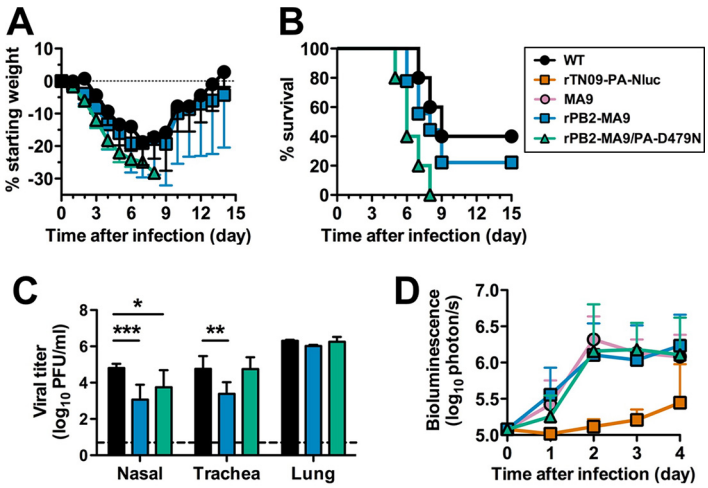

FIG 5 *In vivo* replication, bioluminescence, and virulence of rPB2-MA9 and rPB2-MA9/PA-D479N in DBA/2 mice. Groups of 5 DBA/2 mice were intranasally inoculated with 30 μl PBS containing 750 PFU of virus, and experiments were repeated. (A and B) Body weight changes (A) and survival (B) were observed for 14 days in intact mice. (C) Virus tissue titers in nasal turbinates, trachea, and lungs were measured 4 dpi. (D) Noninvasive bioluminescence intensities in the lungs were observed for 4 days in intact mice. The reported values are means and standard deviations. (A and B) The data are cumulative from three independent experiments ($n = 15$). (C and D) The data are from two experiments ($n = 10$). *, $P < 0.05$; **, $P < 0.01$; ***, $P < 0.001$.

PB2-MA9 in the virus rPB2-MA9/PA-D479N restored virus replication to wild-type-like levels in MDCK cells, mouse lungs, and mouse trachea (in DBA/2 and BALB/c strains) but not in nasal tissue (Fig. 4C and 5C). Compared to the wild type, rPB2-MA9/PA-D479N caused similar weight loss in BALB/c mice and increased weight loss in DBA/2 mice (Fig. 5A and 6A). In DBA/2 mice, the wild type caused 60% mortality, while rPB2-MA9/PA-D479N caused 100% mortality (Table 2 and Fig. 5B); 100% of BALB/c mice survived infection with either the wild type or rPB2-MA9/PA-D479N (data not shown). With respect to *in vivo* bioluminescence, MA-9, rPB2-MA9, and rPB2-MA9/PA-D479N had similarly high levels that exceeded the level of unadapted rTN09-PA-Nluc by approximately 10-fold (Fig. 5D).

rPB2-MA9/PA-D479N is genetically stable *in vitro* and *in vivo*. To assess the genetic stability of the *Nluc* reporter gene, we performed two experiments. First, we performed reverse transcription (RT)-PCR using primers that flanked the engineered region of the *PA-Nluc* gene to determine whether the entire gene was retained after infection in mice or passage in MDCK or A549 cells. The samples studied included wild-type virus lacking the reporter insertion, rPB2-MA9/PA-D479N passaged between

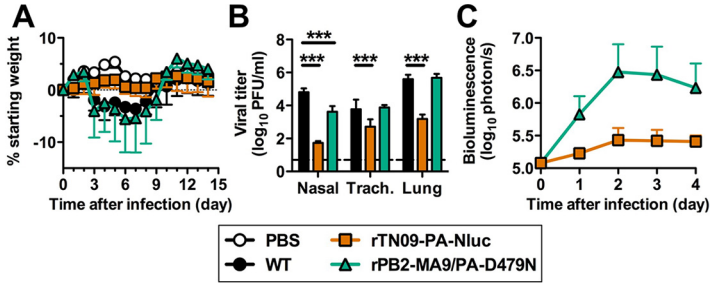

FIG 6 *In vivo* replication, bioluminescence, and weight loss of rPB2-MA9/PA-D479N in BALB/c mice. Groups of 5 BALB/c mice were intranasally inoculated with 30 μl PBS containing 5,000 PFU of virus. (A) Body weight changes were monitored for 14 days. All the animals survived infection. (B) Virus tissue titers in nasal turbinates, trachea, and lungs were measured 4 dpi. (C) Noninvasive bioluminescence intensities in the lungs were observed for 4 days in intact mice. The reported values are means and standard deviations. ***, $P < 0.001$.

TABLE 3 *Nluc* reporter gene stability of rPB2-MA9/PA-D479N after passage

Mouse	Retention of Nluc activity (no. of plaques/total)		
	C1M1[a]	C6M1[b]	C1A5M1[c]
1	9/9	10/10	10/10
2	10/10	10/10	10/10
3	10/10	10/10	10/10
4	10/10	10/10	10/10
5	10/10	10/10	10/10

[a]One passage in MDCK cells and 4 days of infection in DBA/2 mice.
[b]Six passages in MDCK cells and 4 days of infection in DBA/2 mice.
[c]One passage in MDCK cells, 5 passages in A549 cells, and 4 days of infection in DBA/2 mice.

6 and 16 times in MDCK cells (C6, C11, and C16), rPB2-MA9/PA-D479N recovered in MDCK cells and then passaged 5 to 15 more times in A549 cells (C1A5, C1A10, and C1A15), and rPB2-MA9/PA-D479N passaged 6 times in cells and then once in DBA/2 mice (C6M1 and C1A5M1). In each case, the entire reporter gene insertion remained intact after passage (Fig. 4D). Next, we inoculated groups of five DBA/2 mice with rPB2-MA9/PA-D479N previously passaged one time in MDCK cells (C1M1), six times in MDCK cells (C6M1), or one time in MDCK cells and five times in A549 cells (C1A5M1). Four days after infection, we recovered the lungs, homogenized them, and plaque titrated the virus in MDCK cells. From each murine lung sample, we picked 9 or 10 plaques, suspended them in phosphate-buffered saline (PBS), and conducted bioluminescence and plaque titration assays in MDCK cells. Overall, we characterized 49 plaques from 5 mice for the C1M1 passage and 50 plaques from 5 mice for the C6M1 and C1A5M1 passages; 100% of the plaques (149/149) retained luminescence activity (Table 3). Thus, rPB2-MA9/PA-D479N retained its reporter gene activity after passage in cell culture and after 4 days of infection in mice.

Adaptive mutations compensate for decreased viral RNA (vRNA) and cRNA yields by increased mRNA production. We first examined the effects of PB2 and PA mutations on polymerase activity by minigenome assay, which measures the collective efficiency of virus genome replication and transcription. We transfected 293T cells with pHW2000 plasmids (39) containing full-length A/TN/1-560/2009 NP, PB1, mutant PB2, and mutant PA gene segments. We also transfected the reporter plasmid pPolI-358Luc, which contains the firefly luciferase open reading frame (ORF) and the cRNA promoter of A/WSN/33 virus *NP* inserted into the pPolI vector (40). Polymerase activity by TN09-PA-Nluc (containing unadapted NP, PB1, PB2, and PA-Nluc gene segments) was 73% that of the wild type at 33°C and measured at 81% and 110% that of the wild type in two independent experiments at 37°C (Fig. 7). In each case, differences between TN09-PA-Nluc and the wild type were not statistically significant ($P > 0.05$). The mutant PB2-E158G and double mutant PB2-E158G/PA-D479N significantly ($P < 0.05$) decreased polymerase activity, reaching a level $<2/3$ that of the wild type at 33°C and $<1/2$ that of the wild type at 37°C. The low polymerase activity of these mutants was consistent with our failure in 10 attempts to rescue rPB2-E158G and the pronounced attenuation of rPB2-E158G/PA-D479N in DBA/2 mice (Table 2). PB2-MA9 (containing the E158G mutation, in addition to C1161T and C1977T silent mutations), which enhanced virus replication and pathogenicity *in vivo*, was found to significantly increase polymerase activity in the minigenome assay to 390% and 370% that of the wild type at 33°C and 37°C, respectively ($P < 0.001$) (Fig. 7). Comparing the seven combinations of mutations in PB2-MA9 revealed that the silent mutation C1161T was largely responsible for the increase in polymerase activity (Fig. 7C). On its own or in combination with PB2-MA9, the PA-D479N mutation contributed to a small increase in polymerase activity at 33°C but to a decrease at 37°C (Fig. 7A and B).

Next, we infected 293T cells with the wild type, rPB2-MA9, or rPB2-MA9/PA-D479N and measured the kinetics of vRNA, cRNA, and mRNA production by real-time RT-PCR. After 3 h of infection, rPB2-MA9 and rPB2-MA9/PA-D479N had vRNA, cRNA, and mRNA levels similar to those of the wild type (Fig. 8). After 6 h of infection, both rPB2-MA9 and

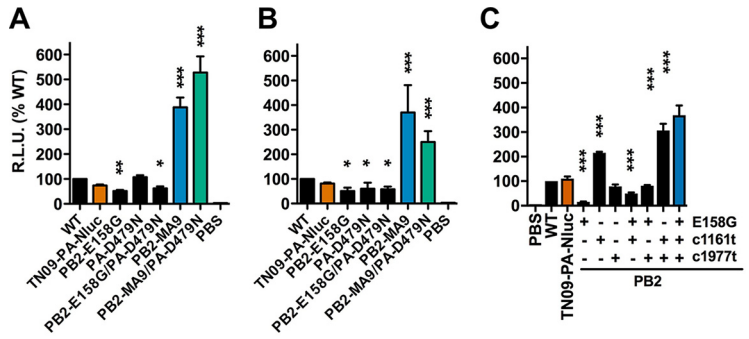

FIG 7 PB2 and PA mutational effects on viral polymerase activity by minigenome assay. 293T cells were transfected with plasmids encoding PA, PB1, PB2, and NP, together with pPolI-358Luc and pβ-gal. Wild-type PB1 and NP plasmids from A/TN/1-560/09 were used in each group, while PB2 and PA plasmids carrying mutants identified in MA9-22 were varied. (A and B) After 24-h incubation at 33°C (A) and 37°C (B), both luciferase and β-Gal expression levels were measured. β-Gal expression was used to normalize the data. R.L.U., relative light units. (C) PB2 mutants carrying nonsynonymous and/or synonymous mutations from MA9-22 were compared at 37°C. The reported values are means and standard deviations from 3 independent experiments ($n = 9$). *, $P < 0.05$; **, $P < 0.01$; ***, $P < 0.001$.

rPB2-MA9/D479N had lower levels of replication (vRNA and cRNA production). After 9 and 12 h of infection, rPB2-MA9 had mRNA levels at 150 and 250% those of the wild type, respectively ($P < 0.001$). The effect was more pronounced for rPB2-MA9/PA-D479N, which had elevated mRNA production earlier (130% after 6 h) and a 12-h level of 510%, significantly higher than those of the wild type and rPB2-MA9 ($P < 0.001$). Thus, the mutant virus with the greatest restoration of replicative and virulence properties in DBA/2 mice also had the greatest increase in mRNA production, despite having decreased vRNA and cRNA production due to reporter gene insertion in the PA gene segment. To determine if the noncoding mutations decreased PB2 protein expression by reducing the stability of *PB2* mRNA, we performed Western blot analyses after 3, 6, 9, or 12 h of infection in 293T cells with WT, rTN09-PA-Nluc, rPB2-MA9/PA-

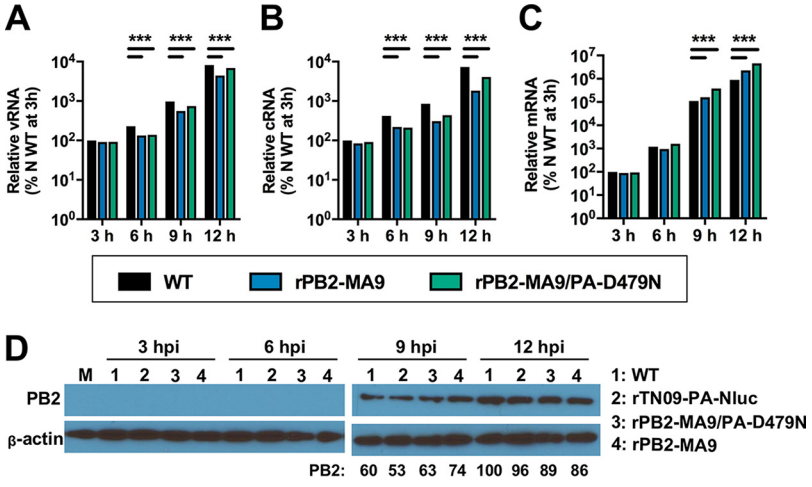

FIG 8 Kinetics of vRNA, cRNA, and mRNA production by rPB2-MA9 and rPB2-MA9/PA-D479N. 293T cells were infected with the wild type, rPB2-MA9, and rPB2-MA9/PA-D479N at an MOI of 3.0 PFU/cell. Total RNA was isolated at 3, 6, 9, and 12 h postinfection. vRNA (A), cRNA (B), and mRNA (C) were quantified by real-time RT-PCR using specific primers annealing to the *NP* gene. The reported values are means and standard deviations of the results of 3 independent experiments ($n = 9$) for the WT, rPB2-MA9, and rPB2-MA9/PA-D479N. ***, $P < 0.001$. (D) PB2 protein expression quantified by Western blotting. 293T cells were infected at an MOI of 3 PFU/cell with WT (lanes 1), rTN09-PA-Nluc (lanes 2), rPB2-MA9/PA-D479N (lanes 3), or rPB2-MA9 (lanes 4) and maintained at 37°C. Cell lysates were harvested at 3, 6, 9, and 12 h postinfection (hpi) and analyzed by Western blotting. β-Actin was used as a loading control. Densitometric values, shown under the 9- and 12-hpi gel, were normalized to the intensity of the WT at 12 hpi. M, mock-infected cell lysate.

D479N, or rPB2-MA9 (Fig. 8D). PB2 protein was detectable after 9 h of infection, at which time the unadapted reporter virus rTN09-PA-Nluc had reduced PB2 expression compared to the WT and the mouse-adapted viruses had increased PB2 expression. However, differences in PB2 expression between the viruses after 12 h were minimal. This suggests PB2 noncoding mutations exert an effect primarily independent of PB2 protein expression.

DISCUSSION

Attenuation of reporter viruses remains an obstacle to noninvasive imaging in animal models. In this work, wild-type-like lung replication and virulence were restored to a luciferase-expressing pH1N1 influenza A virus by directed evolution in murine lungs that maximized the bioluminescence-to-titer ratio during each round of selection. Unadapted rTN09-PA-Nluc was attenuated approximately 10-fold for replication *in vitro* and *in vivo*, causing substantially less weight loss and mortality in DBA/2 mice. Mouse-adapted virus after 9 passages (MA-9) had an ~10-fold increased bioluminescence signal and restored *in vivo* fitness. Isolation of MA-9 clones and reconstruction of reverse genetics variants harboring single and multiple mutations revealed that the adapted reporter virus was enhanced by a combination of PA-D479N and PB2-E158G amino acid mutations, along with the PB2 noncoding mutation C1161T. Minigenome and real-time RT-PCR assays showed that these mutations increased mRNA transcription. In addition to having enhanced replication, virulence, and bioluminescence in both DBA/2 and BALB/c mice, rPB2-MA9/PA-D479N was genetically stable for reporter gene expression after 16 passages in cell culture and after 6 passages in cell culture followed by 4 days of infection in mice. Overall, these studies demonstrate directed evolution is an effective approach to restoring reporter virus fitness; they also describe a pH1N1 virus, rPB2-MA9/PA-D479N, that may be useful in future noninvasive imaging studies.

Similar to rTN09-PA-Nluc, other unadapted luciferase-expressing influenza reporter viruses were attenuated (10, 11, 13–15, 17, 35). For example, similarly constructed viruses containing Nluc insertions in the PA genes of A/WSN/33 (H1N1) and A/California/04/2009 (H1N1) replicated to levels ~10-fold lower *in vitro* at early (~12-h) time points and ~5-fold lower in the lungs of mice (13, 15, 16, 35). Such relatively mild attenuation by reporter viruses lacking further adaptation should be considered a bioengineering success, even if they could be further improved by adaptation. *Gaussia* and firefly luciferase insertions into the NA, PB2, or PA gene of A/PR/8/34 (H1N1) caused 10- to 100-fold lower replication *in vitro* and in mice, resulting in 50% mouse lethal dose (MLD_{50}) values ≥50-fold higher than those of the corresponding wild-type virus (10, 14, 17). Finally, the replication rate of B/Yamagata/16/1988 in MDCK cells was reduced 5- to 10-fold; *in vivo* properties were not reported (11).

The RNA-dependent RNA polymerase of influenza viruses is a nanomachine consisting of PB1, PB2, and PA proteins that have polymerase-catalytic, cap-binding, and cap endonuclease activities, respectively (41, 42). The PB2 mutation E158G, identified here and in two previous mouse adaptations of pH1N1 (43, 44), is located near the N terminus of α-helix 9, which forms a lid over the polymerase channel (41) (Fig. 9). The lid is thought to function as a gatekeeper that directs primer (cap) entry into the channel after PA-catalyzed cleavage while simultaneously preventing newly synthesized product from becoming degraded by the PA catalytic domain during its exit from the polymerase channel in the opposite direction from the template (45). The E158G mutation may alter gatekeeper efficiency either by shortening α-helix 9 or, more likely, by removing the negatively charged sidechain, as an E158A mutation also enhances pathogenicity in mice (43).

Despite enhancing polymerase activity in the context of rPB2-MA9/PA-D479N, a single E158G mutation in the background of TN09-PA-Nluc decreased polymerase activity in the minigenome assay, and we were unsuccessful in generating by reverse genetics in 10 attempts a single PB2-E158G mutation in the background of rTN09-PA-Nluc. In contrast, a single E158G mutation in the contexts of A/CA/04/2009 and A/New

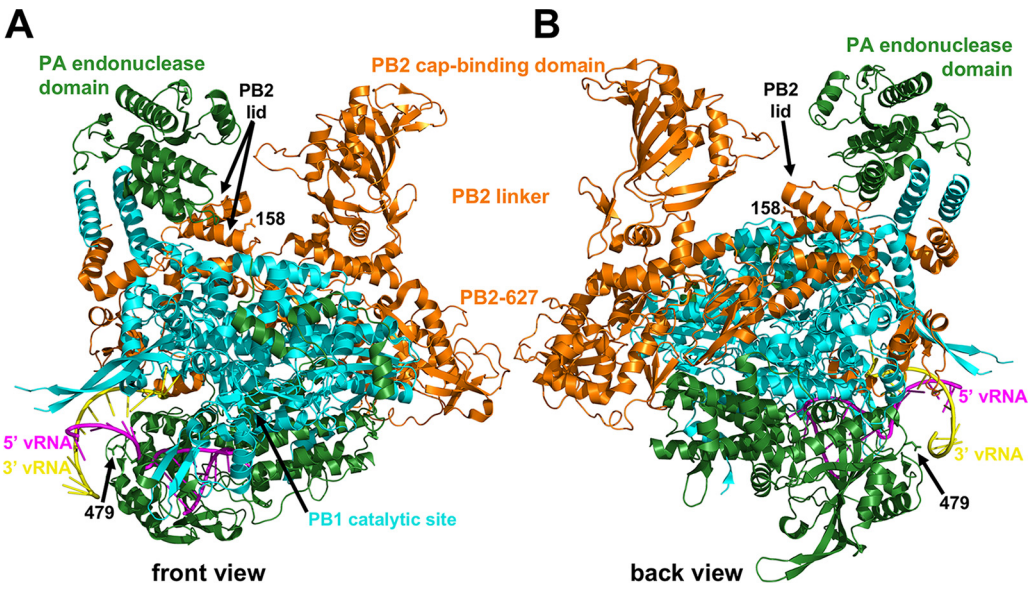

FIG 9 Polymerase structure and locations of mouse-adaptive mutations. Shown are front (A) and back (B) views of the polymerase complex from A/little yellow-shouldered bat/Guatemala/060/2010 (H17N10) (PDB accession no. 4WSB) (41). The proteins are identified by maintaining the original color conventions for PA (green), PB2 (orange), and PB1 (cyan). The PA endonuclease, PB2 cap-binding, PB2 linker, PB2-627, PB2 lid, and PB1 catalytic-site domains are labeled. Residues PA-D479 (479) and PB2-E158 (158) are the only residues for which sidechains are shown. 5′ (magenta) and 3′ (yellow) viral RNAs are also shown. PA-D479 is positioned at the bottom of a rim that funnels up into the polymerase channel. PB2-E158 is located in an α-helical lid that directs newly captured caps down into the PB1 catalytic site and prevents newly synthesized RNA from being cleaved by the PA endonuclease domain when it exits the top of the polymerase.

York/1682/2009 enhanced polymerase activity in minigenome assays and increased fitness in mice (43, 44). Thus, the functional consequence of PB2-E158G appears to be isolate specific. As PB2-E158G enhanced replication in the backgrounds of A/CA/04/2009 and A/New York/1682/2009 but was deleterious in the background of rTN09-PA-Nluc, a known mouse-adaptive mutation engineered in the context of one strain may not always yield a beneficial outcome when introduced into a different strain. Despite being more laborious, the unbiased approach of serial passage may provide an advantage over engineering previously identified mutations into reporter viruses in some cases. While PB2-E158G favors virus replication in mice, the mutation is most likely unfavored in other species, as only 3 out of 9,746 known H1N1 PB2 sequences from 2009 to 2017 contain this polymorphism (http://fludb.org). The three isolates are A/red-winged tinamou/Argentina/MP1/2008 (46), A/swine/Hong Kong/NS2761/2010 (47), and mouse-adapted A/Tomsk/273-MA3/2010 (gi:675440788).

PA residue 479 is located in a short loop connecting α-helix 17 and β-strand 17 in the C-terminal domain (PA-C) (41, 45). PA479 and its loop are positioned at the periphery of the rim of the wide channel through which the template strand enters the complex and the synthesized strand exits, making no apparent protein-protein or protein-RNA contacts (Fig. 9). It is unknown whether PA-D479N increases polymerase activity by altering interactions with entering/exiting RNA strands or via interactions with host cell proteins on a host-specific basis. Only 5 out of 9,390 known H1N1 PA sequences from 2009 to 2017 contain the D479N polymorphism (gi:558483952, 291094384, 485086210,649789084, and 649788606), and only 11 other mutations of the highly prevalent aspartic acid residue have been observed.

The synonymous PB2 mutation C1161T increased polymerase activity 2-fold in the minigenome assay and contributed to enhanced virus replication by rPB2-MA9/PA-D479N. Among 9,746 H1N1 PB2 nucleotide sequences from 2009 to 2017 (http://fludb.org) at position 1161, cytosine and thymine represent 71.4% and 28.5% of the sequences, respectively. With respect to codon usage, AGT and AGC have similar relative synonymous codon usage (RSCU) values of 1.204 and 1.126, respectively, for

pdmH1N109 viruses (48). Therefore, this substitution is unlikely to be responsible for increasing RNA polymerase activity due to codon usage. Nucleotide 1161 is distant from the flanking promoter and packaging sequences. Instead, it is positioned in the center of the PB2 sequence, which totals 2,280 nucleotides, at the boundary of a predicted RNA secondary structure consisting of conserved residues 1041 to 1160 (49). The C1161T mutation is estimated by RNAfold (50) to have a $\Delta\Delta G$ of -1.6 kcal/mol; thus, it may enhance polymerase activity by stabilizing RNA secondary structure. Additional studies beyond the scope of this work would be needed to confirm this possibility or to explore other mechanisms by which nucleotide 1161 enhances polymerase activity.

We are unaware of any other luciferase-expressing influenza reporter virus restored to wild-type levels of replication and virulence in mice. Venus enhanced green fluorescent protein (eGFP) was inserted into the NS gene segments of A/PR/8/1934 (H1N1) and A/Viet Nam/1203/2004 (H5N1), and the viruses were mouse adapted by blind passage (22, 36, 51). As in the present study, virulence-enhancing mutations in mouse-adapted Venus-H5N1 were mapped to the PB2 and PA genes (i.e., residues V25A and R443K, respectively). PB2 residue 25 is located in a loop between α-helices 2 and 3 in the N-terminal domain, interacting with the PB1 hydrophobic sidechains M711 and A712 located in a short loop between PB1 α-helices 32 and 33 (41). Based on structural considerations, PB2-V25A may enhance viral replication in mice, thereby increasing virulence, by stabilizing PB1-PB2 interactions (36). PA-R443 is located in the PA-C domain in the center of α-helix 16, where it interacts with Q545 in PB1 α-helix 22 (41). Thus, PA-R443K may enhance viral replication and pathogenicity in mice by stabilizing PA-PB2 interactions (36).

Venus-PR8 was enhanced in mice by PB2-E712D and HA-T380A mutations (51). PB2-E712 is highly conserved and is located in the nuclear localization signal (NLS) domain. PB2-E712D may enhance PB2 interactions with importin to increase trafficking to the nucleus or alter interactions with RIG-I or other cellular factors (51). Venus-PR8 residue HA-T380 (H1 numbering) is in HA2 α-helix A (52). The T380A mutation most likely destabilizes interactions between helix A and the central coiled coil formed by the C helices, thereby destabilizing the native hemagglutinin (HA) protein and increasing its activation pH. This apparently enhances Venus-PR8 replication in MDCK cells, but not in mice, suggesting HA-T380A may have been a passenger mutation during mouse adaptation (51).

In the present study, we used a directed-evolution approach that maximized the bioluminescence-to-titer ratio in an attempt to enhance the bioluminescence signal-to-noise ratio and avoid loss of the reporter gene while adapting a pH1N1 virus to mice. The resultant mouse-adapted reporter virus had a 10-fold increase in *in vivo* bioluminescence and was genetically stable. Numerous other pH1N1 viruses not containing reporter genes were adapted to mice by blind passage (43, 44, 53–59). Some of the mutations map to the polymerase complex and were shown to increase polymerase activity (43, 44, 56–59). Thus, blind adaptation could potentially yield a virus that maintains its reporter gene and could even have increased reporter gene expression (36, 51). However, in the 9 studies blind adapting pH1N1 to mice, mutations were mapped to each of the 8 gene segments. This suggests many avenues exist for adapting influenza A viruses to mice, not all of which would optimize reporter gene stability and expression. The results presented here demonstrate the utility of directed evolution when adapting an influenza reporter virus. Additional studies would be needed to directly compare the relative merits and drawbacks of directed versus blinded adaptation.

In summary, we have demonstrated directed evolution as an effective approach to increase the fitness and bioluminescence of an influenza reporter virus in mice. The success of this study encourages the application of directed evolution to adapt other influenza reporter viruses to animal models, such as mice, ferrets, and guinea pigs. Our mechanistic studies revealed that reporter gene insertion decreased vRNA and cRNA synthesis, but in the mouse-adapted variant, fitness was restored by increased tran-

scription due to PB2-E158G and PA-D479N amino acid mutations and *PB2* C1161T and C1977T synonymous mutations. From these studies, we advanced the reporter virus rPB2-MA9/PA-D479N. This Nluc-expressing virus is nonattenuated *in vitro* and in influenza-susceptible (DBA/2) and influenza-resistant (BALB/c) mouse strains, and its signal emitting from living mice is increased 10-fold compared to unadapted rTN09-PA-Nluc. Luciferase-expressing reporter viruses have been used to measure infection levels in living mice (4, 11, 13, 15, 17), the initiation site and extent of respiratory spread after transmission (13, 60, 61), respiratory spread and clearance in an immunocompromised host (62, 63), protective immunity after primary infection or vaccination (13, 35, 60, 61, 64), mechanisms of attenuation (4, 15), hemagglutinin inhibition (HAI) and microneutralization (MN) titers (8, 13, 24, 61), monoclonal antibody efficacy (10, 11), antiviral drug potency (5, 7, 11, 17, 21), and titers of virus stocks (13, 21). Similarly, we expect rPB2-MA9/PA-D479N to be a valuable tool in studying *in vivo* pH1N1 replication, pathogenesis, and virus-host interactions and in characterizing antiviral drugs and vaccines.

MATERIALS AND METHODS

Ethics statement. All animal studies were conducted following the Guide for the Care and Use of Laboratory Animals from the National Research Council of the National Academies of the United States (65). Experiments using mice were approved by the Animal Care and Use Committee of St. Jude Children's Research Hospital (protocol number 464). They were performed in compliance with relevant institutional policies; the Association for the Accreditation of Laboratory Animal Care guidelines; the National Institutes of Health regulations; and local, state, and federal laws. Animals were anesthetized with isoflurane and euthanized with CO_2.

Cells and plasmids. MDCK (ATCC CCL-34), 293T (ATCC CRL-3216), and A549 (ATCC CCL-185) cells were maintained in Dulbecco's modified Eagle's medium (DMEM) supplemented with 10% fetal bovine serum (FBS). TransIT-LT1 (Mirus) was used as the transfection reagent for 293T cells. All cells were incubated at 37°C in 5% CO_2 unless otherwise specified. Plasmids for virus rescue containing cDNA of A/TN/1-560/09 (H1N1) were kindly provided by Richard Webby. Mutations in PB2 and PA were generated by site-directed mutagenesis using QuikChange (Stratagene, La Jolla, CA). All plasmids and mutants were sequenced to confirm the identity and the absence of unwanted mutations by the Hartwell Center for Bioinformatics and Biotechnology at St. Jude Children's Research Hospital. Sequencing results were analyzed using CLC Genomics Workbench 8 software (CLC Bio).

Creation of reporter virus cDNA plasmids. Nluc luciferase was cloned into the 5′ end of the PA gene of A/TN/1-560/09 using a previously described strategy (15). In brief, the ORF of the Nluc coding sequence and a stop codon were fused to the C terminus of the PA gene via an amino acid GSG linker following an autoproteolytic 2A peptide from foot-and-mouth disease virus (66). The last 50 nucleotides from the 5′ end of the PA ORF and the native 5′ untranslated region (UTR) were adjacent after the Nluc stop codon. In addition, 18 silent mutations were introduced into the wobble position at the 5′ end of the PA ORF to avoid undesired splicing. The PA-Nluc segment was synthesized (Epoch Life Science) and subcloned into SalI and NaeI sites of the pHW2000 vector (39). To identify mutations in the mouse-adapted reporter virus MA9-22, RT-PCR was performed to generate cDNA of each gene (primer sequences are available upon request). The cDNAs of PB1, PA, HA, NP, M, and NS were cloned into a pHW2000 vector using the BsmBI site, while the cDNAs of PB2 and NA were cloned into a pHW2000 vector using the BsaI site. Sanger sequencing was performed by the Hartwell Center for Bioinformatics and Biotechnology at St Jude Children's Research Hospital.

Virus rescue, plaque titration, and multistep replication. (i) Virus rescue. Reporter virus was generated by reverse genetics as described previously (39). Briefly, 1 μg of each plasmid was mixed and incubated with 18 μl TransIT-LT (Mirus) in 1 ml Opti-MEM at room temperature for 20 min. The mixture was gently removed to 70 to 90% confluent 293T cells in a 6-well plate. After 8 h, the transfection mixture was replaced with 1.4 ml Opti-MEM plus 0.3% bovine serum albumin (BSA). Twenty-four to 30 h later, 200 μl trypsin was added to the well to reach a final concentration of 0.5 μg/ml. Cells were harvested 46 to 50 h postinfection using scrapers and cocultured with MDCK cells at 50 to 60% confluence. The successful rescue of virus was confirmed by plaque assay, after which recombinant reporter virus was amplified in MDCK cells and the sequence was confirmed by RT-PCR and Sanger sequencing. Viral stocks were split into aliquots and stored at −80°C until needed.

(ii) Plaque titration. MDCK cells were seeded in 6-well plates at a density of 7.5×10^5 24 to 30 h before loading 10-fold dilutions of virus in 500 μl. The cells were agitated every 15 min during incubation at 37°C for 1 h. The cells were then washed with PBS and overlaid with 2.5 ml of minimal essential medium (MEM) containing 0.4% agarose, 0.4% BSA, 0.3% sodium bicarbonate ($NaHCO_3$), 2 mM L-glutamine, 12.5 mg/ml of penicillin, 4 mg/ml of streptomycin, 1× BME vitamin solution (Sigma), and 2 ng/ml tosylsulfonyl phenylalanyl chloromethyl ketone (TPCK) trypsin. The plates were incubated at 37°C for 48 h to allow plaque formation. The cells were fixed in 10% formaldehyde for 2 h and visualized by staining with 0.1% crystal violet.

(iii) Multistep replication. Confluent MDCK cells in T75 flasks were infected with wild-type A/TN/1-560/2009 or mutants at a multiplicity of infection (MOI) of 0.01 PFU/cell. After 1 h of adsorption at 37°C,

the inoculum was removed, and the cells were washed three times with PBS. Fresh infection medium was added, and the infected cells were incubated at 37°C. At different time points postinfection, 0.5 ml of the supernatants was collected and then centrifuged at 3,000 rpm at 4°C for 10 min. The supernatants were collected and stored at −80°C, and the virus titer was determined by plaque assay in MDCK cells.

Mouse adaptation. Groups of five 6-week-old female DBA/2 mice (Jackson Laboratories, Bar Harbor, ME) were used for each round of virus passage. The mice were anesthetized with isoflurane and intranasally inoculated with various viral stocks. After inoculation, bioluminescent imaging was performed daily for 4 days. On day 4 postinoculation, the mice were euthanized with CO_2, and the lungs were collected in 0.5 ml ice-cold PBS and homogenized. Titers were determined by plaque assay in MDCK cells. The lung lysate with the highest bioluminescence-to-titer ratio was used to inoculate 3 DBA/2 mice, and the second-highest one was used to inoculate 2 DBA/2 naive mice. The procedure was repeated for 12 passages. The initial inoculation dose of rTN09-PA-Nluc was 7,500 PFU. Subsequent inoculation doses were stepwise decreased as follows: 5,000 PFU for MA-1/2/3, 1,000 PFU for MA-4/5/6, 200 PFU for MA-7/8/9, and 50 PFU for MA-10/11/12. The inoculum volume was always 30 μl.

***In vivo* virus replication and clinical symptoms.** Groups of five 6-week-old female DBA/2 mice were anesthetized and intranasally inoculated with various viral stocks. Body weight and survival were monitored daily over a period of 14 days. Mice that lost >25% of their original weight were euthanized. Bioluminescence imaging was performed daily for 4 days. Nasal turbinates, trachea, and lungs were harvested on day 4 postinoculation to determine viral titers by plaque assay in MDCK cells. Groups of 5 6-week-old BALB/c female mice were inoculated with 30 μl PBS or 5,000 PFU of the WT, rTN09-PA-Nluc, or rPB2-MA9/PA-D479N. The mice were evaluated daily for morbidity over 14 days. Separate groups were used for daily bioluminescence imaging. At day 4 postinfection, nasal turbinates, trachea, and lungs were harvested so that tissue titers could be measured by plaque assay.

***In vivo* bioluminescence.** For bioluminescence imaging, the hair in the area over the trachea and lungs was removed 3 days before inoculation. Nano-Glo luciferase substrate (Promega) was diluted 1:20 in cold PBS, and each mouse was retro-orbitally injected with 100 μl of the mixture. Daily injections were alternated between eyes. Images were acquired after the injection of substrate using a Xenogen IVIS charge-coupled-device (CCD) camera system (Caliper Life Science). Analyses were performed with Living Image 4.5 software (Caliper Life Sciences). Regions of interest (ROIs) were manually defined to quantify bioluminescence signals. All data were expressed as total flux (photons per second). All data in composite images utilize the same scale.

Reporter gene stability. rPB2-MA9/PA-D479N (C1) was used to infect MDCK and A549 cells at an MOI of 0.01. At 48 h after infection, the culture medium was harvested and centrifuged at 3,000 rpm at 4°C for 20 min, and 100 μl of the clarified supernatant was used to infect the next passage of MDCK or A549 cells in T25 flasks. The supernatant was aliquoted and kept at −80°C. The procedures were repeated 15 times in MDCK (C2 to C16) and A549 (C1A1 to C1A15) cells. TRIzol reagent (Life Technologies) was used for RNA extraction from cell culture viral stocks C6, C11, C16, C1A5, C1A10, and C1A15. RT-PCR was performed on RNA isolated from various viral stocks and mouse lung homogenates 4 days after inoculation of the C1 stock. Two primers specifically targeting the 3′ UTR (5′-TATTCGTCTCAGGGA GCGAAAGCAGGTAC-3′) and 5′ UTR (5′-ATATCGTCTCGTATTAGTAGAAACAAGGTACTT-3′) of PA were used. The PCR products were analyzed by electrophoresis using a 1.0% agarose gel.

To determine the stability of the reporter virus in mice, groups of 5 DBA/2J mice were inoculated with 30 μl containing 50 PFU of rPB2-MA9/PA-D479N passages C1, C6, and C1A5. On day 4 postinoculation, lungs were harvested and homogenized in 0.5 ml ice-cold PBS to yield C1M1, C6M1, and C1A4M1. Plaque purification was performed with MDCK cells in 6-well plates. After 48 h, 10 plaques were picked from each lung homogenate and resuspended in 0.5 ml ice-cold PBS. Two hundred microliters of the suspension mixture was inoculated into MDCK cells in 12-well plates. The remaining 300 μl was used for plaque assays in MDCK cells. After 2 days, Nano-Glo substrate (Promega) was added to each well of 12-well plates for bioluminescence imaging using a Xenogen IVIS camera system (Caliper Life Science). Plaques were also visualized with 0.1% crystal violet.

Minigenome assay. 293T cells at 80 to 90% confluence in 12-well plates were transfected with 0.1 μg pPolI-358Luc (40), 0.1 μg PB1, 0.1 μg PB2, 0.1 μg PA, and 0.2 μg NP plasmids (wild type and mutated). Plasmid pβ-gal, which encodes β-galactosidase (β-Gal), was used as an internal control for the assay. As a negative control, 293T cells were transfected with the same plasmids but without the NP plasmid. At 24 h posttransfection at 37°C or 33°C, the cells were washed with ice-cold PBS and lysed in 200 ml 1× passive lysis buffer in each well. They were then covered with foil and rocked at room temperature for 20 min to achieve full lysis. The lysates were centrifuged at 3,000 rpm for 10 min, and 20 μl supernatant was taken for luciferase and β-galactosidase assays. Firefly luciferase levels of all mutants were determined by luminometer, standardized against β-Gal levels, and normalized to the level of the WT. Each experiment was performed in triplicate.

Real-time RT-PCR. Confluent 293T cells were infected with A/Tennessee/1-560/2009 and each mutant at an MOI of 3 PFU/cell. At 3, 6, 9, and 12 h postinfection, total RNA was isolated from virus-infected cells using TRIzol reagent (Life Technologies). Real-time RT-PCR was performed using SYBR green ER qPCR SuperMix on an ABI 7500 real-time PCR system (Applied Biosystems, Foster City, CA). PCR and cycling parameters were set according to the manufacturer's recommendations. The cycle parameters were 95°C for 2 min and then 40 cycles of 94°C for 15 s for denaturation, 55°C for 30 s for annealing, and 72°C for 15 s for extension. To distinguish between mRNA, vRNA, and cRNA production by real-time RT-PCR, we used primers specific for each species as described previously (67, 68). The primers were NP-vRNAf (5′-GGCCGTCATGGTGGCGAAT-3′), NP-vRNAr (5′-CTCAGAATGAGTGCTGACCGTGCC-3′), NP-cRNAf (5′-GCTAGCTTCAGCTAGGCATC-3′), NP-cRNAr (5′-CGATCGTGCCTTCCTTTG-3′), NP-mRNAf (5′-CCA

GATCGTTCGAGTCGT-3′), and NP-mRNAr (5′-CGATCGTGCCTTCCTTTG-3′). GAPDH (glyceraldehyde-3-phosphate dehydrogenase) was used to normalize viral gene levels with an mGAPDH-f sequence of 5′-ACCACAGTCCATGCCATCA-3′ and an mGAPDH-r sequence of 5′-TCCACCACCCTGTTGCTGT-3′. The RNA expression levels of all the mutants were normalized by the mGAPDH level and compared to that of the wild type using the $\Delta\Delta C_T$ method (69).

Western blotting. 293T cells were infected at an MOI of 3 with WT and recombinant reporter viruses. Cell lysates were harvested after 3, 6, 9, and 12 h of incubation at 37°C. The cell lysates were resolved by 4 to 12% Bis-Tris gels, and protein bands were transferred to polyvinylidene difluoride (PVDF) membranes by wet electroblotting. The membranes were blocked with 5% (wt/vol) skimmed milk powder in PBST (PBS containing 0.2% Tween 20) for 2 h at room temperature. Next, the membranes were washed with PBST and incubated overnight at 4°C with anti-influenza A virus PB2 monoclonal antibody at a 1:2,000 dilution (GenScript; A01464-40). The membranes were extensively washed with PBST and incubated at room temperature for 1 h with anti-rabbit horseradish peroxidase-conjugated secondary antibody. Protein expression was normalized using beta-actin (Abcam; ab8224) as a loading control.

Statistical analyses. Virus yields in cell culture, weight changes of mice, virus titers in lungs, polymerase activities, bioluminescent signals, and RT-PCR were compared by analysis of variance (ANOVA) with GraphPad Prism5 software. *P* values of <0.05 were considered statistically significant.

Structural analyses. Structures were visualized using MacPyMOL (PyMOL Molecular Graphics System v1.5.0.5 enhanced for Mac OS X; Schrödinger, LLC). Protein Data Bank (PDB) accession no. 4WSB (Bat Flu A) and its coloring conventions were used (45).

ACKNOWLEDGMENTS

We thank Megan Shaw for kindly providing the pPolI-358Luc plasmid and Richard Webby for kindly providing the pH1N1 reverse genetics plasmids. We thank Marion Russier and Guohua Yang for helpful discussions and advice. We thank Heba Mostafa and Prady Baviskar for assistance with bioluminescence-imaging experiments and Jeremy Jones and Mark Zanin for helpful technical assistance on minigenome experiments. We thank the St. Jude Animal Resources Center and the Hartwell Center for Bioinformatics and Biotechnology for sequencing.

Meisui Liu was supported in part by grant R25CA23944 from the National Cancer Institute. This work was funded, in part, by the National Institute of Allergy and Infectious Diseases under Centers of Excellence for Influenza Research and Surveillance (CEIRS) contract no. HHSN272201400006C, the Children's Infection Defense Center (CIDC) at St. Jude Children's Research Hospital, and the American Lebanese Syrian Associated Charities (ALSAC).

REFERENCES

1. Hutchens M, Luker GD. 2007. Applications of bioluminescence imaging to the study of infectious diseases. Cell Microbiol 9:2315–2322. https://doi.org/10.1111/j.1462-5822.2007.00995.x.
2. Rostad CA, Currier MC, Moore ML. 2016. Fluorescent and bioluminescent reporter myxoviruses. Viruses 8:E214. https://doi.org/10.3390/v8080214.
3. Falzarano D, Groseth A, Hoenen T. 2014. Development and application of reporter-expressing mononegaviruses: current challenges and perspectives. Antiviral Res 103:78–87. https://doi.org/10.1016/j.antiviral.2014.01.003.
4. Burke CW, Mason JN, Surman SL, Jones BG, Dalloneau E, Hurwitz JL, Russell CJ. 2011. Illumination of parainfluenza virus infection and transmission in living animals reveals a tissue-specific dichotomy. PLoS Pathog 7:e1002134. https://doi.org/10.1371/journal.ppat.1002134.
5. Rameix-Welti MA, Le Goffic R, Herve PL, Sourimant J, Remot A, Riffault S, Yu Q, Galloux M, Gault E, Eleouet JF. 2014. Visualizing the replication of respiratory syncytial virus in cells and in living mice. Nat Commun 5:5104. https://doi.org/10.1038/ncomms6104.
6. Hasan MK, Kato A, Shioda T, Sakai Y, Yu D, Nagai Y. 1997. Creation of an infectious recombinant Sendai virus expressing the firefly luciferase gene from the 3′ proximal first locus. J Gen Virol 78:2813–2820. https://doi.org/10.1099/0022-1317-78-11-2813.
7. Yan D, Weisshaar M, Lamb K, Chung HK, Lin MZ, Plemper RK. 2015. Replication-competent influenza virus and respiratory syncytial virus luciferase reporter strains engineered for co-infections identify antiviral compounds in combination screens. Biochemistry 54:5589–5604. https://doi.org/10.1021/acs.biochem.5b00623.
8. Fuentes S, Crim RL, Beeler J, Teng MN, Golding H, Khurana S. 2013. Development of a simple, rapid, sensitive, high-throughput luciferase reporter based microneutralization test for measurement of virus neutralizing antibodies following Respiratory Syncytial Virus vaccination and infection. Vaccine 31:3987–3994. https://doi.org/10.1016/j.vaccine.2013.05.088.
9. Shaw ML, Palese P. 2013. Orthomyxoviridae, p 1151–1185. *In* Knipe DM, Howley PM (ed), Fields virology, 6th ed. Lippincott Williams and Wilkins, Philadelphia, PA.
10. Heaton NS, Leyva-Grado VH, Tan GS, Eggink D, Hai R, Palese P. 2013. In vivo bioluminescent imaging of influenza A virus infection and characterization of novel cross-protective monoclonal antibodies. J Virol 87:8272–8281. https://doi.org/10.1128/JVI.00969-13.
11. Fulton BO, Palese P, Heaton NS. 2015. Replication-competent influenza B reporter viruses as tools for screening antivirals and antibodies. J Virol 89:12226–12231. https://doi.org/10.1128/JVI.02164-15.
12. Munier S, Rolland T, Diot C, Jacob Y, Naffakh N. 2013. Exploration of binary virus-host interactions using an infectious protein complementation assay. Mol Cell Proteomics 12:2845–2855. https://doi.org/10.1074/mcp.M113.028688.
13. Karlsson EA, Meliopoulos VA, Savage C, Livingston B, Mehle A, Schultz-Cherry S. 2015. Visualizing real-time influenza virus infection, transmission and protection in ferrets. Nat Commun 6:6378. https://doi.org/10.1038/ncomms7378.
14. Spronken MI, Short KR, Herfst S, Bestebroer TM, Vaes VP, van der Hoeven B, Koster AJ, Kremers GJ, Scott DP, Gultyaev AP, Sorell EM, de Graaf M, Barcena M, Rimmelzwaan GF, Fouchier RA. 2015. Optimisations and challenges involved in the creation of various bioluminescent and fluorescent influenza A virus strains for in vitro and in vivo applications. PLoS One 10:e0133888. https://doi.org/10.1371/journal.pone.0133888.
15. Tran V, Moser LA, Poole DS, Mehle A. 2013. Highly sensitive real-time in vivo imaging of an influenza reporter virus reveals dynamics of replica-

tion and spread. J Virol 87:13321–13329. https://doi.org/10.1128/JVI.02381-13.
16. Tran V, Poole DS, Jeffery JJ, Sheahan TP, Creech D, Yevtodiyenko A, Peat AJ, Francis KP, You S, Mehle A. 2015. Multi-modal imaging with a toolbox of influenza A reporter viruses. Viruses 7:5319–5327. https://doi.org/10.3390/v7102873.
17. Pan W, Dong Z, Li F, Meng W, Feng L, Niu X, Li C, Luo Q, Li Z, Sun C, Chen L. 2013. Visualizing influenza virus infection in living mice. Nat Commun 4:2369. https://doi.org/10.1038/ncomms3369.
18. Pena L, Sutton T, Chockalingam A, Kumar S, Angel M, Shao H, Chen H, Li W, Perez DR. 2013. Influenza viruses with rearranged genomes as live-attenuated vaccines. J Virol 87:5118–5127. https://doi.org/10.1128/JVI.02490-12.
19. Sutton TC, Obadan A, Lavigne J, Chen H, Li W, Perez DR. 2014. Genome rearrangement of influenza virus for anti-viral drug screening. Virus Res 189:14–23. https://doi.org/10.1016/j.virusres.2014.05.003.
20. Breen M, Nogales A, Baker SF, Martinez-Sobrido L. 2016. Replication-competent influenza A viruses expressing reporter genes. Viruses 8:E179. https://doi.org/10.3390/v8070179.
21. Eckert N, Wrensch F, Gartner S, Palanisamy N, Goedecke U, Jager N, Pohlmann S, Winkler M. 2014. Influenza A virus encoding secreted Gaussia luciferase as useful tool to analyze viral replication and its inhibition by antiviral compounds and cellular proteins. PLoS One 9:e97695. https://doi.org/10.1371/journal.pone.0097695.
22. Fukuyama S, Katsura H, Zhao D, Ozawa M, Ando T, Shoemaker JE, Ishikawa I, Yamada S, Neumann G, Watanabe S, Kitano H, Kawaoka Y. 2015. Multi-spectral fluorescent reporter influenza viruses (Color-flu) as powerful tools for in vivo studies. Nat Commun 6:6600. https://doi.org/10.1038/ncomms7600.
23. Lakdawala SS, Wu Y, Wawrzusin P, Kabat J, Broadbent AJ, Lamirande EW, Fodor E, Altan-Bonnet N, Shroff H, Subbarao K. 2014. Influenza A virus assembly intermediates fuse in the cytoplasm. PLoS Pathog 10:e1003971. https://doi.org/10.1371/journal.ppat.1003971.
24. Li F, Feng L, Pan W, Dong Z, Li C, Sun C, Chen L. 2010. Generation of replication-competent recombinant influenza A viruses carrying a reporter gene harbored in the neuraminidase segment. J Virol 84:12075–12081. https://doi.org/10.1128/JVI.00046-10.
25. Manicassamy B, Manicassamy S, Belicha-Villanueva A, Pisanelli G, Pulendran B, Garcia-Sastre A. 2010. Analysis of in vivo dynamics of influenza virus infection in mice using a GFP reporter virus. Proc Natl Acad Sci U S A 107:11531–11536. https://doi.org/10.1073/pnas.0914994107.
26. Martinez-Sobrido L, Cadagan R, Steel J, Basler CF, Palese P, Moran TM, Garcia-Sastre A. 2010. Hemagglutinin-pseudotyped green fluorescent protein-expressing influenza viruses for the detection of influenza virus neutralizing antibodies. J Virol 84:2157–2163. https://doi.org/10.1128/JVI.01433-09.
27. Nogales A, Baker SF, Martinez-Sobrido L. 2015. Replication-competent influenza A viruses expressing a red fluorescent protein. Virology 476:206–216. https://doi.org/10.1016/j.virol.2014.12.006.
28. Ozawa M, Victor ST, Taft AS, Yamada S, Li C, Hatta M, Das SC, Takashita E, Kakugawa S, Maher EA, Neumann G, Kawaoka Y. 2011. Replication-incompetent influenza A viruses that stably express a foreign gene. J Gen Virol 92:2879–2888. https://doi.org/10.1099/vir.0.037648-0.
29. Tokusumi T, Iida A, Hirata T, Kato A, Nagai Y, Hasegawa M. 2002. Recombinant Sendai viruses expressing different levels of a foreign reporter gene. Virus Res 86:33–38. https://doi.org/10.1016/S0168-1702(02)00047-3.
30. Kato A, Kiyotani K, Hasan MK, Shioda T, Sakai Y, Yoshida T, Nagai Y. 1999. Sendai virus gene start signals are not equivalent in reinitiation capacity: moderation at the fusion protein gene. J Virol 73:9237–9246.
31. Touzelet O, Loukili N, Pelet T, Fairley D, Curran J, Power UF. 2009. De novo generation of a non-segmented negative strand RNA virus with a bicistronic gene. Virus Res 140:40–48. https://doi.org/10.1016/j.virusres.2008.10.019.
32. Liang Y, Hong Y, Parslow TG. 2005. *cis*-Acting packaging signals in the influenza virus PB1, PB2, and PA genomic RNA segments. J Virol 79:10348–10355. https://doi.org/10.1128/JVI.79.16.10348-10355.2005.
33. Dos Santos Afonso E, Escriou N, Leclercq I, van der Werf S, Naffakh N. 2005. The generation of recombinant influenza A viruses expressing a PB2 fusion protein requires the conservation of a packaging signal overlapping the coding and noncoding regions at the 5′ end of the PB2 segment. Virology 341:34–46. https://doi.org/10.1016/j.virol.2005.06.040.
34. Hall MP, Unch J, Binkowski BF, Valley MP, Butler BL, Wood MG, Otto P, Zimmerman K, Vidugiris G, Machleidt T, Robers MB, Benink HA, Eggers CT, Slater MR, Meisenheimer PL, Klaubert DH, Fan F, Encell LP, Wood KV. 2012. Engineered luciferase reporter from a deep sea shrimp utilizing a novel imidazopyrazinone substrate. ACS Chem Biol 7:1848–1857. https://doi.org/10.1021/cb3002478.
35. Czako R, Vogel L, Lamirande EW, Bock KW, Moore IN, Ellebedy AH, Ahmed R, Mehle A, Subbarao K. 2017. In vivo imaging of influenza virus infection in immunized mice. mBio 8:e00714-17. https://doi.org/10.1128/mBio.00714-17.
36. Zhao D, Fukuyama S, Yamada S, Lopes TJ, Maemura T, Katsura H, Ozawa M, Watanabe S, Neumann G, Kawaoka Y. 2015. Molecular determinants of virulence and stability of a reporter-expressing H5N1 influenza A virus. J Virol 89:11337–11346. https://doi.org/10.1128/JVI.01886-15.
37. Iuliano AD, Roguski KM, Chang HH, Muscatello DJ, Palekar R, Tempia S, Cohen C, Gran JM, Schanzer D, Cowling BJ, Wu P, Kyncl J, Ang LW, Park M, Redlberger-Fritz M, Yu H, Espenhain L, Krishnan A, Emukule G, van Asten L, Pereira da Silva S, Aungkulanon S, Buchholz U, Widdowson MA, Bresee JS, Global Seasonal Influenza-Associated Mortality Collaborator N. 2018. Estimates of global seasonal influenza-associated respiratory mortality: a modelling study. Lancet 391:1285–1300. https://doi.org/10.1016/S0140-6736(17)33293-2.
38. Memoli MJ, Morens DM, Taubenberger JK. 2008. Pandemic and seasonal influenza: therapeutic challenges. Drug Discov Today 13:590–595. https://doi.org/10.1016/j.drudis.2008.03.024.
39. Hoffmann E, Webster RG. 2000. Unidirectional RNA polymerase I-polymerase II transcription system for the generation of influenza A virus from eight plasmids. J Gen Virol 81:2843–2847. https://doi.org/10.1099/0022-1317-81-12-2843.
40. Hoffmann HH, Palese P, Shaw ML. 2008. Modulation of influenza virus replication by alteration of sodium ion transport and protein kinase C activity. Antiviral Res 80:124–134. https://doi.org/10.1016/j.antiviral.2008.05.008.
41. Pflug A, Guilligay D, Reich S, Cusack S. 2014. Structure of influenza A polymerase bound to the viral RNA promoter. Nature 516:355–360. https://doi.org/10.1038/nature14008.
42. Obayashi E, Yoshida H, Kawai F, Shibayama N, Kawaguchi A, Nagata K, Tame JR, Park SY. 2008. The structural basis for an essential subunit interaction in influenza virus RNA polymerase. Nature 454:1127–1131. https://doi.org/10.1038/nature07225.
43. Ilyushina NA, Khalenkov AM, Seiler JP, Forrest HL, Bovin NV, Marjuki H, Barman S, Webster RG, Webby RJ. 2010. Adaptation of pandemic H1N1 influenza viruses in mice. J Virol 84:8607–8616. https://doi.org/10.1128/JVI.00159-10.
44. Zhou B, Li Y, Halpin R, Hine E, Spiro DJ, Wentworth DE. 2011. PB2 residue 158 is a pathogenic determinant of pandemic H1N1 and H5 influenza A viruses in mice. J Virol 85:357–365. https://doi.org/10.1128/JVI.01694-10.
45. Reich S, Guilligay D, Pflug A, Malet H, Berger I, Crepin T, Hart D, Lunardi T, Nanao M, Ruigrok RW, Cusack S. 2014. Structural insight into cap-snatching and RNA synthesis by influenza polymerase. Nature 516:361–366. https://doi.org/10.1038/nature14009.
46. Alvarez P, Mattiello R, Rivailler P, Pereda A, Davis CT, Boado L, D'Ambrosio E, Aguirre S, Espinosa C, La Torre J, Donis R, Mattion N. 2010. First isolation of an H1N1 avian influenza virus from wild terrestrial non-migratory birds in Argentina. Virology 396:76–84. https://doi.org/10.1016/j.virol.2009.10.009.
47. Liang H, Lam TT, Fan X, Chen X, Zeng Y, Zhou J, Duan L, Tse M, Chan CH, Li L, Leung TY, Yip CH, Cheung CL, Zhou B, Smith DK, Poon LL, Peiris M, Guan Y, Zhu H. 2014. Expansion of genotypic diversity and establishment of 2009 H1N1 pandemic-origin internal genes in pigs in China. J Virol 88:10864–10874. https://doi.org/10.1128/JVI.01327-14.
48. Fancher KC, Hu W. 2011. Codon bias of influenza A viruses and their hosts. Am J Mol Biol 1:174–182. https://doi.org/10.4236/ajmb.2011.13017.
49. Moss WN, Priore SF, Turner DH. 2011. Identification of potential conserved RNA secondary structure throughout influenza A coding regions. RNA 17:991–1011. https://doi.org/10.1261/rna.2619511.
50. Mathews DH, Disney MD, Childs JL, Schroeder SJ, Zuker M, Turner DH. 2004. Incorporating chemical modification constraints into a dynamic programming algorithm for prediction of RNA secondary structure. Proc Natl Acad Sci U S A 101:7287–7292. https://doi.org/10.1073/pnas.0401799101.
51. Katsura H, Fukuyama S, Watanabe S, Ozawa M, Neumann G, Kawaoka Y. 2016. Amino acid changes in PB2 and HA affect the growth of a recombinant influenza virus expressing a fluorescent reporter protein. Sci Rep 6:19933. https://doi.org/10.1038/srep19933.

52. Wilson IA, Skehel JJ, Wiley DC. 1981. Structure of the hemagglutinin membrane glycoprotein of influenza-virus at 3-A resolution. Nature 289:366–373. https://doi.org/10.1038/289366a0.
53. Park S, Il Kim J, Lee I, Bae JY, Yoo K, Nam M, Kim J, Sook Park M, Song KJ, Song JW, Kee SH, Park MS. 2017. Adaptive mutations of neuraminidase stalk truncation and deglycosylation confer enhanced pathogenicity of influenza A viruses. Sci Rep 7:10928. https://doi.org/10.1038/s41598-017-11348-0.
54. Prokopyeva EA, Sobolev IA, Prokopyev MV, Shestopalov AM. 2016. Adaptation of influenza A(H1N1)pdm09 virus in experimental mouse models. Infect Genet Evol 39:265–271. https://doi.org/10.1016/j.meegid.2016.01.022.
55. Sakabe S, Ozawa M, Takano R, Iwastuki-Horimoto K, Kawaoka Y. 2011. Mutations in PA, NP, and HA of a pandemic (H1N1) 2009 influenza virus contribute to its adaptation to mice. Virus Res 158:124–129. https://doi.org/10.1016/j.virusres.2011.03.022.
56. Seyer R, Hrincius ER, Ritzel D, Abt M, Mellmann A, Marjuki H, Kuhn J, Wolff T, Ludwig S, Ehrhardt C. 2012. Synergistic adaptive mutations in the hemagglutinin and polymerase acidic protein lead to increased virulence of pandemic 2009 H1N1 influenza A virus in mice. J Infect Dis 205:262–271. https://doi.org/10.1093/infdis/jir716.
57. Ye J, Sorrell EM, Cai Y, Shao H, Xu K, Pena L, Hickman D, Song H, Angel M, Medina RA, Manicassamy B, Garcia-Sastre A, Perez DR. 2010. Variations in the hemagglutinin of the 2009 H1N1 pandemic virus: potential for strains with altered virulence phenotype? PLoS Pathog 6:e1001145. https://doi.org/10.1371/journal.ppat.1001145.
58. Yu Z, Cheng K, Sun W, Zhang X, Li Y, Wang T, Wang H, Zhang Q, Xin Y, Xue L, Zhang K, Huang J, Yang S, Qin C, Wilker PR, Yue D, Chen H, Gao Y, Xia X. 2015. A PB1 T296R substitution enhance polymerase activity and confer a virulent phenotype to a 2009 pandemic H1N1 influenza virus in mice. Virology 486:180–186. https://doi.org/10.1016/j.virol.2015.09.014.
59. Zhu W, Zhu Y, Qin K, Yu Z, Gao R, Yu H, Zhou J, Shu Y. 2012. Mutations in polymerase genes enhanced the virulence of 2009 pandemic H1N1 influenza virus in mice. PLoS One 7:e33383. https://doi.org/10.1371/journal.pone.0033383.
60. Burke CW, Bridges O, Brown S, Rahija R, Russell CJ. 2013. Mode of parainfluenza virus transmission determines the dynamics of primary infection and protection from reinfection. PLoS Pathog 9:e1003786. https://doi.org/10.1371/journal.ppat.1003786.
61. Burke CW, Li M, Hurwitz JL, Vogel P, Russell CJ. 2015. Relationships among dissemination of primary parainfluenza virus infection in the respiratory tract, mucosal and peripheral immune responses, and protection from reinfection: a noninvasive bioluminescence-imaging study. J Virol 89:3568–3583. https://doi.org/10.1128/JVI.03581-14.
62. Mostafa HH, Vogel P, Srinivasan A, Russell CJ. 2016. Non-invasive imaging of Sendai virus infection in pharmacologically immunocompromised mice: NK and T cells, but not neutrophils, promote viral clearance after therapy with cyclophosphamide and dexamethasone. PLoS Pathog 12:e1005875. https://doi.org/10.1371/journal.ppat.1005875.
63. Mostafa HH, Vogel P, Srinivasan A, Russell CJ. 2018. Dynamics of Sendai virus spread, clearance, and immunotherapeutic efficacy after hematopoietic cell transplant imaged noninvasively in mice. J Virol 92:e01705-17. https://doi.org/10.1128/JVI.01654-17.
64. Phan SI, Chen Z, Xu P, Li Z, Gao X, Foster SL, Teng MN, Tripp RA, Sakamoto K, He B. 2014. A respiratory syncytial virus (RSV) vaccine based on parainfluenza virus 5 (PIV5). Vaccine 32:3050–3057. https://doi.org/10.1016/j.vaccine.2014.03.049.
65. National Research Council Committee for the Update of the Guide for the Care and Use of Laboratory Animals. 2011. Guide for the Care and Use of Laboratory Animals, 8th ed. The National Academies Press, Washington, DC. https://doi.org/10.17226/12910.
66. Donnelly ML, Hughes LE, Luke G, Mendoza H, ten Dam E, Gani D, Ryan MD. 2001. The 'cleavage' activities of foot-and-mouth disease virus 2A site-directed mutants and naturally occurring '2A-like' sequences. J Gen Virol 82:1027–1041. https://doi.org/10.1099/0022-1317-82-5-1027.
67. Kawakami E, Watanabe T, Fujii K, Goto H, Watanabe S, Noda T, Kawaoka Y. 2011. Strand-specific real-time RT-PCR for distinguishing influenza vRNA, cRNA, and mRNA. J Virol Methods 173:1–6. https://doi.org/10.1016/j.jviromet.2010.12.014.
68. Elbahesh H, Cline T, Baranovich T, Govorkova EA, Schultz-Cherry S, Russell CJ. 2014. Novel roles of focal adhesion kinase in cytoplasmic entry and replication of influenza A viruses. J Virol 88:6714–6728. https://doi.org/10.1128/JVI.00530-14.
69. Livak KJ, Schmittgen TD. 2001. Analysis of relative gene expression data using real-time quantitative PCR and the 2(-Delta Delta C(T)) method. Methods 25:402–408. https://doi.org/10.1006/meth.2001.1262.